communications earth & environment

Article

A Nature Portfolio journal

https://doi.org/10.1038/s43247-025-03083-6

Triassic–Jurassic environmental instability on the subtropical eastern Tethyan margin linked to low-latitude dinosaur dispersal

Check for updates

Jianbo Chen[1], Yi-Ning Niu[1], Rongyao Ma[1], Yan-Ling Zhou[1], Wen-Jie Liu[1], Ya-Ming Wang[2], Hai-Lu You[3], Xing Xu[1,3], Shu-Zhong Shen[4] & Zhuo Feng[1,5]

The Triassic–Jurassic transition marks a critical interval, witnessing major biotic turnovers, including the rise of dinosaurs and the end-Triassic mass extinction, triggered by the Central Atlantic Magmatic Province. However, the volcanism linked to terrestrial ecosystem disturbance and dinosaur distribution remains poorly constrained. Here we present an integrated dataset of chemostratigraphic and astrochronological records for a continental drill core from the Kunming Basin in Yunnan Province of Southwest China, where rich dinosaur assemblages have been previously identified. Three negative carbon isotope excursions coupled with volcanogenic mercury anomalies confirm pulsed volcanism-induced environmental impacts on this subtropical terrestrial setting and placement of the Triassic–Jurassic boundary. Critically, the earliest regional sauropodomorph fossils occurred at ~200.17 Ma, indicating post-extinction colonization in low palaeolatitudes by medium- to large-bodied dinosaurs. Large-scale volcanism-induced stressors, potentially coupled with increased climate seasonality, likely created ecological opportunities facilitating dinosaur expansion in the earliest Jurassic.

The Triassic–Jurassic transition (TJT; ~201 Ma) represents one of the most critical intervals in Earth's history, marked by profound environmental upheaval and a fundamental reshaping of the biosphere. It witnessed the catastrophic end-Triassic mass extinction (ETME), one of the Phanerozoic's "Big Five" biotic crises, largely attributed to the emplacement of the Central Atlantic Magmatic Province (CAMP). This large-scale volcanic activity, linked to the stepwise disintegration of the Pangea supercontinent[1], directly or indirectly released vast quantities of greenhouse gases (e.g., >5×10^{12} tons CO_2), triggering climate warming, oceanic acidification, and severe disruption of the global carbon cycle, which triggered the collapse in both marine and terrestrial ecosystems[2–5]. Yet, amidst this catastrophe, a remarkable evolutionary success unfolded: Dinosaurs originated in regional Carnian (early Late Triassic) assemblages and achieved global dominance by the Early Jurassic, although the mechanisms that drove this transition remain debated[6–10]. This apparent paradox – mass extinction coinciding with the ascendancy of a major clade – raises critical questions: Did the environmental stressors that caused the EPME also create the opportunities that facilitated the dinosaurs' rise, particularly their expansion into the low-latitude western Tethys?

While extensive marine records document the TJT environmental perturbations through characteristic carbon isotope excursions (CIEs) and mercury (Hg) anomalies indicative of CAMP volcanism[11–15], our understanding of the terrestrial realm lags significantly, which is exacerbated by a geographic bias, with most high-resolution TJT records clustered in North American and European basins (e.g., Newark Basin, St. Audries's Bay), leaving a large portion of Pangean landmasses poorly documented. East Asian terrestrial sequences, particularly the dinosaur-rich Jurassic strata of Yunnan Province, Southwest China[16–18], offer an exceptional yet under-

[1]State Key Laboratory for Vegetation Structure, Functions and Construction (VegLab), Institute of Palaeontology, Yunnan Key Laboratory of Earth System Science, Yunnan University, Kunming, 650500, China. [2]The Geological Museum of China, Beijing, 100034, China. [3]Key Laboratory of Vertebrate Evolution and Human Origins, Institute of Vertebrate Paleontology and Paleoanthropology, Chinese Academy of Sciences, Beijing, 100044, China. [4]State Key Laboratory for Mineral Deposits Research, School of Earth Sciences and Engineering, and Frontiers Science Center for Critical Earth Material Cycling, Nanjing University, Nanjing, 210023, China. [5]Southwest United Graduate School, Kunming, 650092, China. e-mail: zhuofeng@ynu.edu.cn

exploited window into this critical transition. The recent discovery of *Wudingloong* in Wuding County, Chuxiong Prefecture of Yunnan, represents the stratigraphically lowest and the earliest diverging sauropodomorph skeletal remains in the Triassic–Jurassic transitional interval that have been found so far in southern China, and possibly East Asia as a whole[19]. It provides a key palaeontological anchor for our study, since its presence is particularly significant, as sauropodomorphs were largely excluded from low palaeolatitudes during the Late Triassic by climatic barriers[10,20]. However, like a previously reported sauropodomorph footprint site in the neighboring Xichang Basin[21], the precise age of this pivotal fossil remains unconstrained. This highlights a broader challenge: correlating terrestrial biotic events with the marine extinction timeline is severely hindered by the typical scarcity of datable volcanic ash layers within continental redbeds.

To overcome these challenges in assessing volcanic forcing and establishing a robust chronostratigraphic framework, we conducted a multi-proxy investigation of a drill core (WK23-1) across the Triassic–Jurassic boundary (TJB) interval in the Wande section of Kunming Basin, Yunnan Province, ~ 1 km away from the locality of the newly discovered sauropodomorph (Fig. 1A). By integrating the high-resolution, coupled organic carbon isotope ($\delta^{13}C_{org}$), mercury chemostratigraphy (Hg concentrations and isotopes), elemental geochemistry, and astronomically-tuned gamma-ray data from the dinosaur-bearing Triassic–Jurassic boundary beds of Southwest China (Fig. 2), this study aims to[1]: refine the TJB placement by correlating characteristic CIEs and Hg anomalies linked to CAMP activity[2]; provide the first age constraints for the earliest sauropodomorph skeletal remains in East Asia. By anchoring the first appearance of a key dinosaur group to a precisely dated record of environmental change, our work provides a direct link between CAMP-driven ecosystem collapse and the subsequent ecological opportunities that fueled one of the most significant evolutionary radiations in Earth's history.

Results

In drill core WK23-1, the Triassic–Jurassic transitional Yubacun Formation is stratigraphically bounded by the overlying Lufeng Formation (Lower Jurassic) at 15.23 m depth and the underlying Shezi Formation (Upper

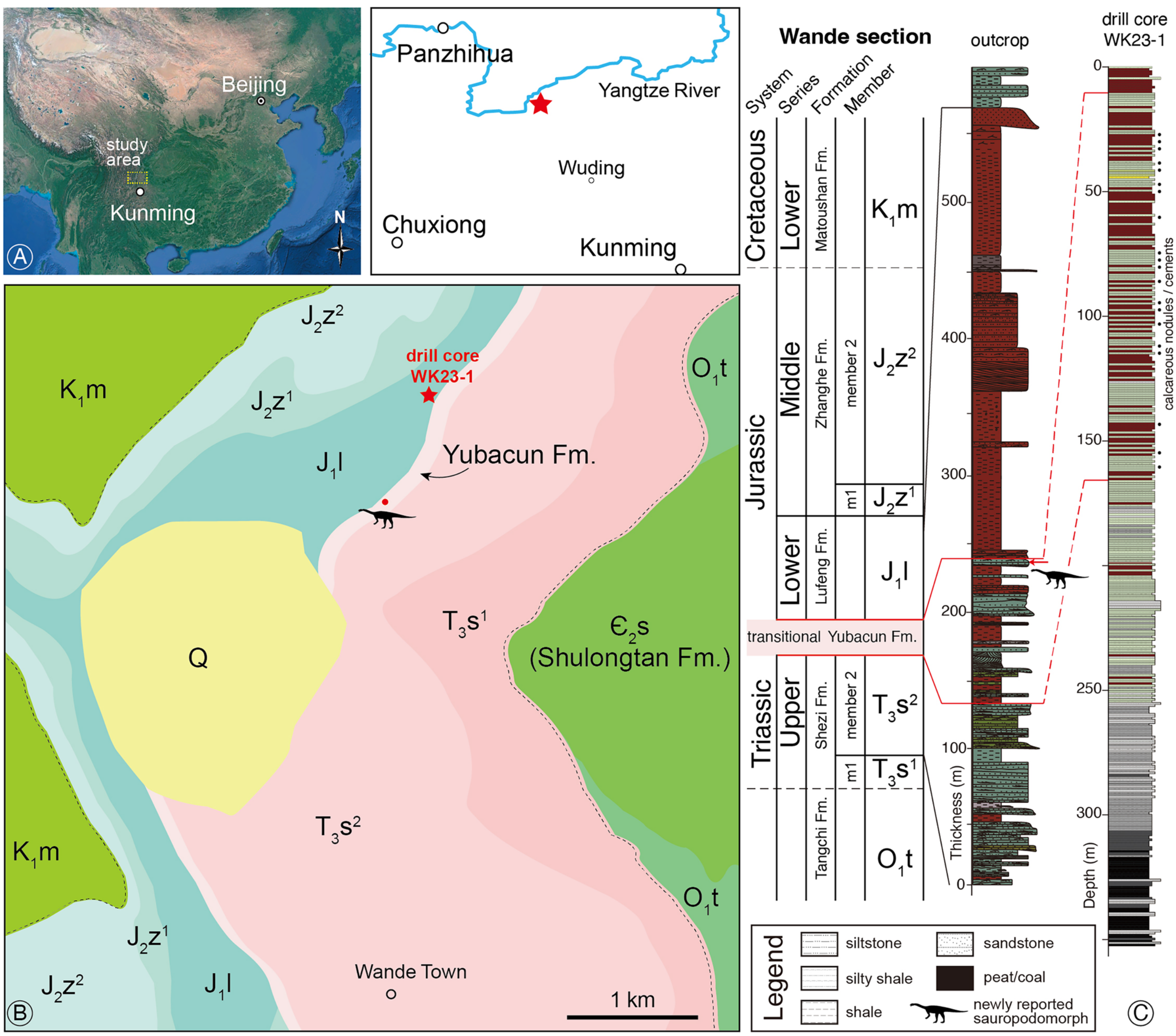

Fig. 1 | Maps and sedimentary sequences of the study area in Southwest China. **A** Geographic location of the study area. **B** Geological map of the study area, revised from the Regional Geological Survey Report by the Yunnan Institute of Geological Survey. **C** Correlation of outcrop and drill core WK23-1 in the Wande section, based on variegated clastic lithology and thickness of the transitional Yubacun Formation. Note: In the drill core, the dinosaur fossils occur no higher than the Shezi–Yubacun boundary at the depth of 15.23 m and no lower than the base of the greyish-green siltstone unit at the depth of 23.73 m, and the Yubacun Formation exhibits an increasing calcareous component upwards, indicating enhanced seasonality upwards the profile (black dots at the far-right of the drill core column).

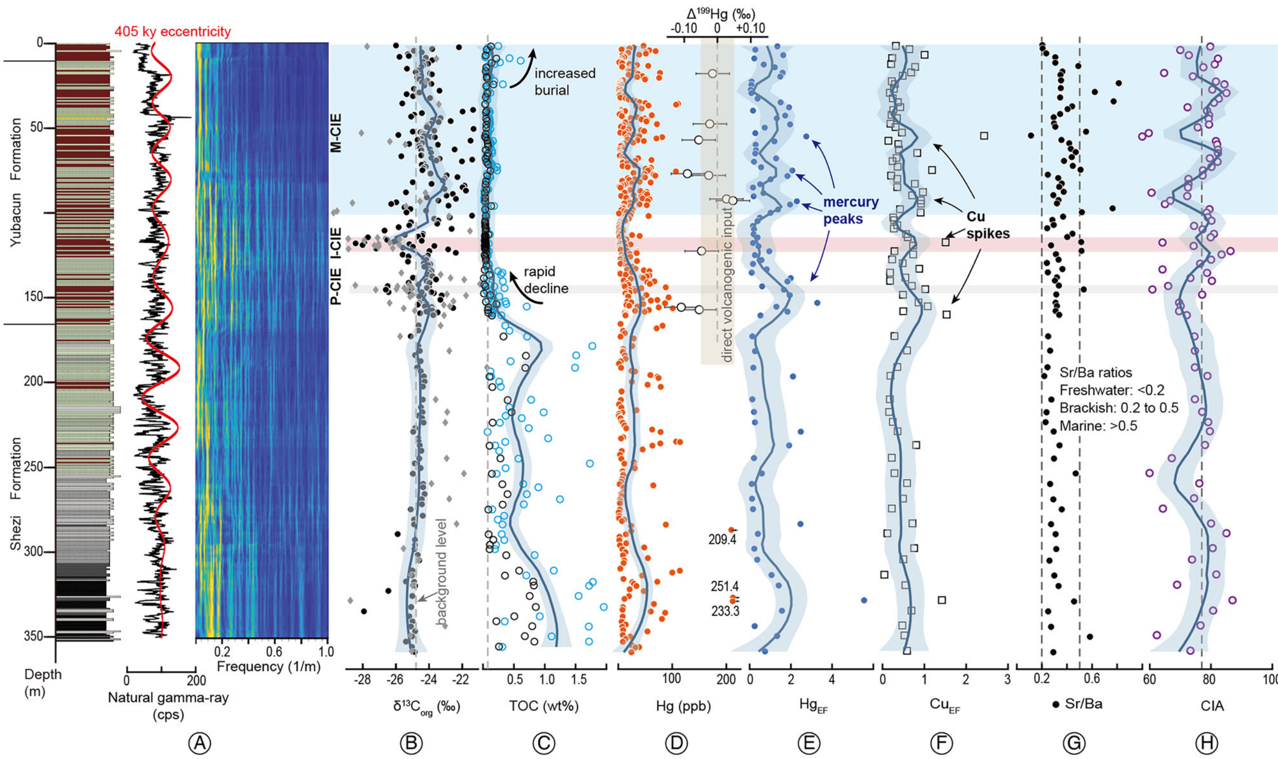

Fig. 2 | Composite framework for reconstructing Triassic–Jurassic transition environmental dynamics recorded in the terrestrial drill core WK23-1. **A** Gamma-ray (GR) data with 405 kyr filtered output and Evolutionary Fast Fourier Transform (FFT) spectrogram of tuned GR data. **B**–**G** Geochemical data including (**B**) $\delta^{13}C_{org}$, (**C**) Total Organic Carbon (TOC), (**D**) Hg concentration (with Hg isotopes insert), (**E**) calculated Hg_{EF}, (**F**) calculated Cu_{EF}, (**G**) palaeosalinity proxy Sr/Ba ratio, and (**H**) Chemical Index of Alteration (CIA). In (**B**), The blue dots and grey diamonds are measurements by Delta V at Yunnan University and MAT 253 at China University of Geosciences (Wuhan), respectively. Grey, pink, and blue rectangles highlight the three CIEs. LOWESS curves (blue line) with 95% confidence intervals (light blue shading) are shown for $\delta^{13}C_{org}$, TOC, Hg, Hg_{EF}, $Cu_{EF,}$ and CIA. The light brown rectangle indicates a potential direct volcanic input characterized by Δ^{199}Hg values of ~0‰.

Triassic) at 157.60 m depth, yielding a total thickness of 142.37 m (Fig. 1B, C; Supplementary Data S1). Astronomical tuning of the gamma-ray series identified more than eight full 405-kyr long-eccentricity cycles, suggesting a total duration of ~3.2 Myrs for the logged core (Fig. 2A). Based on this tuning, the depositional duration of the Yubacun Formation is estimated to be ~1.71 Myrs.

The $\delta^{13}C_{org}$ record reveals a major shift across the TJB. Values in the Upper Triassic Shezi Formation are relatively stable, ranging from -27.9‰ to -23.5‰ (average of -24.7‰, n = 89). In contrast, a pronounced isotopic shift occurs in the Yubacun Formation, with values spanning from -29.8‰ to -20.2‰ (avg. of -24.3‰, n = 217), and features three distinct negative carbon isotope excursions (CIEs)[1]: a "precursor" CIE (P-CIE) occurs between the depth of 142.63 to 146.68 m (duration: ~42 kyrs), characterized by an average of -25.7‰ (n = 16) with values dropping to a minimum of -28.4‰[2]; an "initial" CIE (I-CIE), a transient negative shift (avg. of -26.4‰) (n = 14) between the depth of 114.92–121.49 m (duration: ~70 kyrs), contains the most negative values in the core, reaching a minimum of -28.9‰[3]; a "main" CIE (M-CIE) initiates at 100.19 m and remains low through the upper Yubacun Formation and into the basal Lufeng Formation (Fig. 2B). Based on the background $\delta^{13}C_{org}$ value (-24.5‰, n = 113), defined from the Shezi Formation to the lowest Yubacun Formation (Fig. 2B), the calculated magnitudes of the P-CIE and I-CIE are ~3.9‰ and ~4.4‰, respectively (Supplementary Data S1).

Total organic carbon (TOC) contents show a marked overall decline upwards from the Shezi Formation (avg. of 0.44 wt%, n = 65) to the Yubacun Formation (avg. of 0.05 wt%, n = 158), with a sharp drop near the Shezi–Yubacun formational boundary. A minor increase in TOC (avg. of 0.09 wt%, n = 14) is observed within the basal Lufeng Formation at the top of the drill core (Fig. 2C).

Mercury (Hg) concentrations, evaluated using an enrichment factor (Hg_{EF}), show several distinct anomalous intervals (Fig. 2D, E). The traditional normalization method (such as Hg/TOC) is not utilized in this work mainly because of the negligible correlation between Hg and its potential host phases (Figure S3). Repeated measurements of selected samples have confirmed that the extremely low TOC contents in the upper half of the core are valid, but they create spuriously high Hg/TOC ratios (up to 5118 ppb/wt % at 95.23 m) that are far beyond the range of previously reported reliable values[22]. Therefore, Hg_{EF} is used to avoid these analytical artifacts while accurately identifying Hg enrichment intervals.

Mercury isotope analysis on ten samples from these anomalous zones, shows minimal mass-independent fractionation (MIF denoted as Δ^{199}Hg values). Most Δ^{199}Hg values cluster near zero, ranging from -0.10‰ to +0.04‰ with an average of -0.03‰, a signature consistent with a volcanogenic Hg source (Fig. 2D). Concurrently, the Chemical Index of Alteration (CIA) values (56.55–86.2, avg. of 74.6, $1\sigma = 6.8$, n = 88) indicate consistently moderate chemical weathering throughout the section (Fig. 2H).

Carbon–mercury dynamics: Linking CAMP volcanism to global and regional disturbance

The Triassic–Jurassic transition (TJT) is characterized by a profound disturbance in the global carbon cycle, recorded as characteristic negative carbon isotope excursions (CIEs) in marine and terrestrial sedimentary archives worldwide[1,15]. These CIEs serve as crucial chemostratigraphic tools for correlating the end-Triassic mass extinction (ETME) across different depositional settings, such as the Tethyan, continental Pangean, and Southern hemisphere marine[11,12,23–26]. Our high-resolution $\delta^{13}C_{org}$ record from drill core WK23-1 in the terrestrial Kunming Basin reveals three such

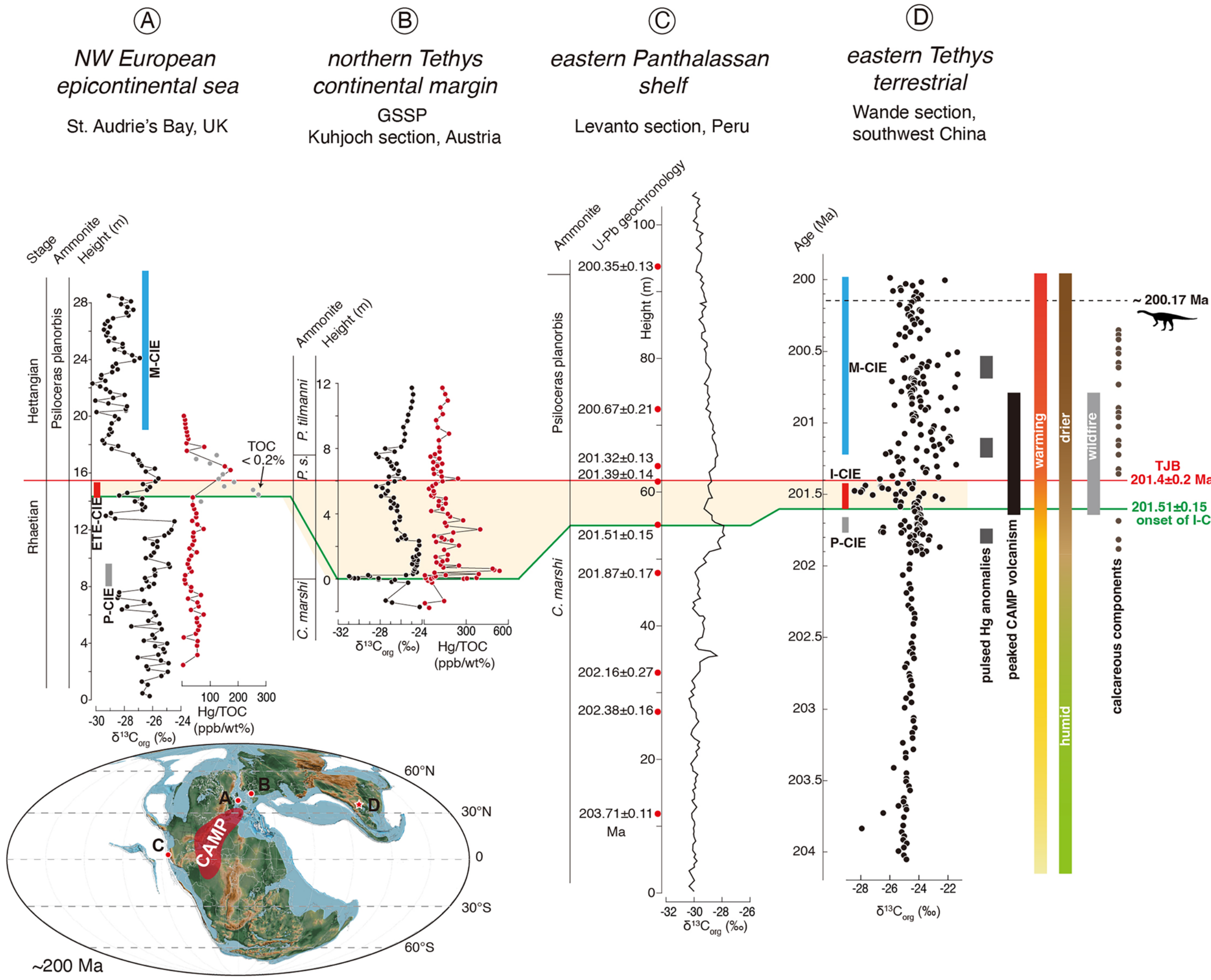

Fig. 3 | Stratigraphic correlation across the Triassic–Jurassic boundary (TJB) between the studied WK23-1 drill core from the Wande section and globally recognized reference sections. The Triassic–Jurassic boundary is marked by the first appearance of the ammonite *Psiloceras spelae* in marine successions. Data compilation for each section includes: (**A**) St. Audrie's Bay (UK): Organic carbon isotopes[11], mercury concentrations[73], and the proposed end-Triassic mass extinction C-isotope excursion (ETE-CIE)[74]. **B** Kuhjoch (Austria): $\delta^{13}C_{org}$ data[12] and Hg data[45]. **C** Levanto (Peru): Composite $\delta^{13}C_{org}$ record and high-precision U-Pb age constraints[32]. **D** Wande section (this study): $\delta^{13}C_{org}$ and pulsed Hg anomaly data (this work), timing of peak Central Atlantic Magmatic Province (CAMP) volcanism[75], evidence for palaeoclimate changes [warming and drier[41]], indications of wildfire events[57], and increased occurrence of calcareous components (this work).

CIEs (termed P-CIE, I-CIE, M-CIE; Fig. 2B), mirroring patterns observed globally. The most prominent of these, the I-CIE, is a sharp negative excursion in our core lasting ~70 kyrs. This duration is comparable to the ~85 kyrs recorded on the Panthalassan margin, in Peru[26], suggesting a remarkably similar pacing for the main environmental crisis on opposite sides of Pangea. While the absolute $\delta^{13}C_{org}$ values are more positive than in marine records from the Panthalassic Ocean and Tethys Ocean, the excursion magnitude of ~4.4‰ is consistent with few other published terrestrial $\delta^{13}C_{org}$ records[11,23–25,27]. Given a predominantly influence by brackish waters suggested by Sr/Ba ratios throughout the core (Fig. 2G), this magnitude of excursion could not be explained by mixing of terrestrial and marine organic carbon[28]. Instead, it likely reflects an enhanced biological fractionation of carbon in response to an intensified hydrological cycle and elevated atmospheric CO_2[2,29]. The global synchronicity of the I-CIE across geographically diverse marine (e.g., Fig. 3A–C) and terrestrial settings [e.g., Junggar Basin[30]] strongly implicates massive injections of volcanic CO_2 and/or thermogenic methane into the ocean-atmosphere system as the primary driver of this worldwide cycle instability[11,23,24]. Anchoring our astrochronological timescale to the established high-precision U-Pb age for the onset of the I-CIE (and thus the ETME) at 201.51 ± 0.15 Ma[31,32], we place this event at 121.49 m depth in our core (Fig. 3D, Supplementary Data S1). Following established correlations where the Triassic–Jurassic boundary (TJB) often slightly post-dates the I-CIE onset[23,32], this allows us to position the TJB at 111.29 m within the transitional Yubacun Formation (Fig. 3D, Figure S1B), providing a critical temporal framework for evaluating biotic and environmental events relative to the extinction horizon.

The direct link to volcanism is further strengthened by our mercury (Hg) data. While many Hg records were documented from marine sections in Europe and North America[13,14], our study provides crucial terrestrial data for the central Yunnan area from the eastern Tethyan realm. The WK23-1 core reveals several distinct Hg enrichment intervals associated with the CIEs (Fig. 2D, E), and the near-zero mass-independent fractionation of these anomalies provides a clear fingerprint of a volcanic source, consistent with the global pattern of pulsed, large-scale volcanic Hg emissions during the TJT[13,14,30,33,34]. This signature arises because volcanic emissions inject primarily Hg(0) into the atmosphere, lacking the significant MIF generated by photochemical reactions involving Hg in the upper atmosphere[35,36].

However, our record also highlights significant regional variability, showing how this global volcanic driver was filtered through local environmental conditions, and reflecting the interplay of global drivers with local factors like organic carbon sources, depositional settings, diagenesis, and regional climate[37–39]. For instance, the P-CIE identified in our drill core, while potentially correlative with events seen in some other sections, lacks clear global synchronicity and thus its status as a truly global signal remains debated[32,40]. In the Kunming Basin, the P-CIE coincides strikingly with a rapid decline in TOC content (Fig. 2B, C), which we interpret as the localized collapse in terrestrial primary productivity or carbon burial. This short-lived negative CIE event (~ 37 kyrs) preceding the main ETME, coupled with the rapid TOC decline at the transition from the Shezi to Yubacun Formation, likely implies the demise of humid peat-forming ecosystems. This interpretation is supported by regional palynological evidence for significant floral turnover, which shows fern-dominated flora (Dipteridaceae/Matoniaceae ferns in the Late Triassic, Cyatheaceae/Dicksoniaceae ferns during the TJT) was replaced by a co-dominance of ferns and cheirolepid conifers in the Early Jurassic across southern China[41]. The drivers could include early CAMP-induced environmental stress, such as aridification or toxic metal loading (Hg, Cu – note the elevated Cu coinciding with the first Hg peak; Fig. 2E, F), synergistically impacting sensitive floras[14,42]. The apparent absence of a distinct P-CIE in many marine sections could further support a predominantly regional hydroclimate or ecosystem control rather than a global atmospheric CO_2 perturbation[32]. Furthermore, the first Hg enrichment (Hg_{EF} up to 3.27) during this precursor event also has a unique, slightly negative Δ^{199}Hg signature (-0.11‰ to -0.05‰), suggesting mobilization of reworked terrestrial Hg from enhanced soil erosion or the combustion of organic-rich soils/sediments during initial environmental upheaval[42–44]. The decoupling of global and local signals is particularly evident during the I-CIE, which, despite being the largest carbon isotope shift, lacks a corresponding Hg peak. We hypothesize that during this interval of peak environmental stress, local changes in the depositional environment—such as shifts in redox conditions or the type of organic matter—reduced the efficiency of Hg scavenging and burial. Thus, even with a probable increase in atmospheric Hg from CAMP, the signal was not effectively preserved, a phenomenon that has been documented at numerous key TJT sections (e.g., St. Audries Bay, New York Canyon[45]) and records associated with other Phanerozoic mass extinctions[46]. High sedimentation rates in the I-CIE interval (Figure S1) could be a possible reason due to the dilution effect[46].

The regional disturbance is also apparent in the character of the "main" CIE (M-CIE) and the weathering proxy record. The M-CIE in WK23-1 appears somewhat muted and prolonged compared to sharp, pronounced excursions seen in some marine records[1], potentially reflecting differences in organic matter sources, degradation pathways, or depositional redox conditions influencing $\delta^{13}C_{org}$ preservation in this terrestrial setting[37,38]. In addition, the CIA values remain relatively stable (56.5–86.2, avg. of 74.6, $1\sigma = 6.8$) throughout the studied interval, indicating persistently moderate chemical weathering intensity in the source area (Fig. 2G). This relative stability contrasts with evidence for extreme climatic fluctuations and potentially intense weathering shifts inferred from proxies in the basins to the north of Kunming Basin, such as Junggar Basin[47,48] or Sichuan Basin[49]. While seemingly indicative of climatic stability, the CIA primarily reflects the intensity of chemical weathering of silicate minerals in the source area over longer timescales. It does not preclude significant changes in other climatic parameters like precipitation seasonality, frequency of extreme events (e.g., droughts, wildfires), or temperature fluctuations, especially in a subtropical setting potentially buffered from the most extreme weathering regime shifts seen at higher latitudes[50]. Therefore, the stable CIA suggests a relatively consistent baseline weathering regime but does not rule out other forms of climate change impacting the ecosystem.

Post-extinction emergence of sauropodomorph dinosaurs in Southwest China: Timing and environmental context

Against the background of global volcanic catastrophe and regionally variable environmental responses, the TJT interval witnessed a crucial moment in vertebrate history: the rise of dinosaurs to ecological dominance[6,7]. A key biogeographic model, the "diachronous rise of dinosaurs" hypothesis, posits that groups like sauropodomorphs originated in mid-palaeolatitudes of Gondwana and were initially confined there during the Carnian and early Norian (Late Triassic) by harsh, arid climates in the palaeotropics[51], and then a northward breakout and dispersal only became feasible around the mid-Norian following climatic amelioration, which produced a cosmopolitan distribution by the Triassic–Jurassic transition. However, as the recent review by Upchurch and Chiarenza[10] makes clear, this picture is nuanced and subject to ongoing debate: Challenges to the "diachronous rise of dinosaurs" hypothesis include the discovery of potential Carnian-age dinosaurs in Laurasia and growing evidence that many early dinosaurs, particularly theropods, already possessed physiological adaptations suitable for arid conditions[52]. Late Triassic sauropodomorphs, by contrast, appear to have been restricted to cooler climates, potentially due to a combination of factors including heat stress associated with larger body size, insufficient plant productivity in arid zones, and direct competition with incumbent pseudosuchian herbivores in the tropics[52,53]. Consistent with this, extensive fieldwork has yielded no confirmed Late Triassic sauropodomorph skeletal remains from the lower palaeolatitudes of southwestern China, potentially due to these environmental filters or geographic barriers[10,54], alongside geological preservation conditions and palaeogeographic configuration of landmasses.

Our astrochronologically-calibrated age model provides the first precise timing for the arrival of sauropodomorphs in this region. We place the sauropodomorph *Wudingloong* fossil horizon (occurring ~15.23 to 23.73 m depth in the topmost Yubacun Formation) at approximately ~200.17 Ma (Figs. 3D and S1). This age is unequivocally Early Jurassic, falling ~1.23 million years after the TJB (placed at 111.29 m, 201.4 Ma based on tuning relative to I-CIE onset at 201.51 Ma). This provides the first direct, time-calibrated evidence that sauropodomorphs colonized Southwest China in the aftermath of the end-Triassic mass extinction.

The timing of this faunal expansion coincides with the recovery interval following the I-CIE and encompasses the M-CIE. While the precise environmental drivers facilitating dinosaur ascendancy remain under investigation[55,56], the environmental stressors associated with CAMP volcanism likely played a complex role. The recurrent mercury spikes aligned with $\delta^{13}C_{org}$ shifts in our record serve as proxies for pulsed volcanic activity and associated environmental perturbations impacting the Kunming Basin during the TJT (Fig. 3). These perturbations, potentially including toxic metal loading (Hg, Cu), climatic instability (though perhaps buffered in terms of weathering intensity), increased aridity or seasonality, and potentially more frequent wildfires fueled by stressed vegetation[57,58], could have selectively disadvantaged contemporaneous faunas and disrupted established ecosystems on land. This disruption may have created ecological opportunities ("vacant niches") for resilient and adaptable groups like dinosaurs[7]. The prolonged environmental instability, potentially reflected in the extended duration of the M-CIE, might have favored taxa capable of coping with fluctuating resources or conditions, although the specific adaptations benefiting early sauropodomorphs require further investigation. The modest recovery of TOC during the M-CIE interval (Fig. 2C) might signal the beginnings of ecosystem reorganization and ameliorated plant productivity upon which these large herbivores arrived and flourished[10].

This post-extinction dispersal into Southwest China likely occurred within a broader context of global climate change. Tectonic activity related to Pangea's fragmentation altered oceanic and atmospheric circulation, while elevated atmospheric CO_2 levels drove overall warming and potentially enhanced climate variability and seasonality[59,60]. Evidence for increased seasonality, even under high CO_2, comes from findings like lake ice-rafted debris in the high-latitude Junggar Basin[9]. The increased occurrence of carbonate nodules or concretions up-section within the drill core suggests that at least transient arid conditions (and therefore seasonality) were becoming more prevalent across the TJT into the earliest Jurassic in the subtropics (Figs. 1C and S2). Such shifts towards more seasonal climates could have profoundly impacted vegetation structure across various latitudes[41,61], potentially transforming previously less favorable habitats (perhaps persistently warm and humid) into landscapes (e.g., more open woodlands or savanna-like ecosystems) accessible or exploitable by large herbivores like sauropodomorphs. While the stable CIA values in the

Kunming Basin suggest the source area weathering intensity did not undergo the dramatic swings seen elsewhere[47–49], increased seasonality in local precipitation patterns or temperature ranges could still have driven significant ecological shifts relevant to faunal turnover and migration, without necessarily altering the bulk silicate weathering signal captured by CIA. Thus, the arrival of sauropodomorphs in Southwest China around 200.17 Ma likely reflects a combination of post-extinction ecological opportunity and adaptation to evolving Early Jurassic climates, particularly the emergence of potentially more seasonal environments across former environmental barriers[56].

Broader implications for terrestrial extinction

Our time-constrained record provides a key opportunity to test models of marine versus terrestrial extinction timing and provide a clear and robust timeline for the aftermath of the crisis. Increasingly, records are starting to show that the marine extinction is associated with early influences of the eruption and ocean acidification and deoxygenation associated with the CO_2 pulses (see review from[1]). Meanwhile, the terrestrial record has been hypothesized to show evidence of a slower reaction, with an initial environmental disruption followed by a slower takeover by dinosaurs following this degradation event, as long-term warming occurs due to increases in CO_2. Our high-resolution data suggest a nuanced scenario: The initial terrestrial ecosystem collapse was synchronous with the earliest CAMP pulses, and the subsequent ecological recovery and establishment of a dinosaur-dominated fauna was a protracted, million-year process.

Our record captures a short-lived (~ 37 kyrs) precursor carbon isotope excursion (P-CIE) that precedes the main global extinction horizon. This event is tightly coupled with a sharp drop in organic carbon (TOC) and a mercury (Hg) spike with a clear terrestrial signature (negative Δ^{199}Hg values). We interpret this as a collapse of the local Late Triassic peat-forming ecosystem, directly triggered by the initial phases of CAMP volcanism. This initial collapse is followed by the larger, globally recognized I-CIE, which is synchronous with the main marine extinction event[1]. This indicates that the terrestrial environment was already severely stressed before or during the primary marine crisis. However, our strongest and most unequivocal conclusion concerns the protracted nature of the subsequent ecological recovery: the first appearance of the sauropodomorph *Wudingloong* occurred more than 1.3 million years after the onset of the main I-CIE extinction event. This provides direct, time-calibrated evidence that the establishment of new, dinosaur-dominated ecosystems was not an immediate rebound. Instead, it was a prolonged recovery period that lasted well over a million years.

Conclusions

This study provides a high-resolution, astrochronologically-calibrated chemostratigraphic record for the terrestrial Triassic–Jurassic transition in Kunming Basin, Southwest China. Our integrated, multi-proxy chemostratigraphic data ($\delta^{13}C_{org}$, Hg concentrations, and Hg isotopes) and astrochronology from drill core WK23-1 document the environmental impact of pulsed Central Atlantic Magmatic Province (CAMP) volcanism through three distinct carbon isotope excursions (CIEs) and associated Hg anomalies. These global signals were also influenced by regional factors, reflected in localized ecosystem shifts linked to the P-CIE and TOC decline, potential terrestrial Hg reworking, and a relatively stable weathering intensity baseline (indicated by CIA) despite inferred climate shifts elsewhere. This new astrochronological framework established the Yubacun Formation's duration (~ 1.71 Myrs) and placed the Triassic–Jurassic boundary (TJB, 201.4 Ma) at 111.29 m depth. Critically, the precise dating of the earliest sauropodomorph skeletal fossils in this region to ~200.17 Ma (Early Jurassic, ~1.23 Myrs post-TJB) demonstrates the post-ETME colonization of the (sub)tropical eastern Tethys by these large herbivores.

Our findings demonstrate that the end-Triassic mass extinction, driven by CAMP volcanism, was instrumental in removing the incumbent terrestrial competitors, leaving ecological niches vacant. The intense, repeated environmental instability we document in the Yubacun Formation—evidenced by the sharp carbon isotope excursions and coupled mercury anomalies—represents a high-resolution local signature of the kill mechanism that drove this global faunal turnover. This volcanic-induced crisis acted as a critical environmental filter, eliminating established groups and creating the ecological opportunity that allowed dinosaurs to cross former climatic barriers. Therefore, our record does not merely coincide with the appearance of sauropodomorphs like *Wudingloong* in this region; it documents the precise environmental upheaval that facilitated the final phase of the "diachronous rise of dinosaurs", enabling the global radiation of dinosaurs that characterized the Jurassic period.

Therefore, this research fills a critical geographic gap in TJT terrestrial records and validates the efficacy of applying multi-proxy chemo- and cyclostratigraphy for high-resolution dating in continental sequences. It provides crucial, time-calibrated context for understanding the interplay between catastrophic volcanism, environmental crisis, ecosystem recovery, and the early diversification dynamics of dinosaurs in a key, previously underexplored region.

Methods

Geological background

The Kunming Basin in Yunnan Province, Southwest China (Fig. 1A), situated within the Tethyan tectonic domain, preserves a critical terrestrial stratigraphic succession across the Triassic–Jurassic transition (TJT). The studied interval encompasses three formations (Fig. 1B, C): The Upper Triassic Shezi Formation, the transitional Yubacun Formation, and the Lower Jurassic Lufeng Formation, in ascending order, which collectively record a continuum of depositional responses to evolving basin dynamics and climatic regimes.

The Shezi Formation is assigned to the Norian–Rhaetian (Late Triassic) based on the presence of the *Yunnanophorus–Indosinion* bivalve zone and the *Dictyophyllum–Clathropteris* plant assemblage[62]. The overlying Yubacun Formation, considered the primary Triassic–Jurassic transitional unit, consists of variegated clastic rocks dominated by grey, greyish-green, and greyish-yellow sandstone intercalated with purplish-red siltstone or mudstone. Palynological assemblages constrain its deposition in the TJT interval[63]. The dinosaur fossils recovered from the uppermost Yubacun Formation at this locality have recently been described as the new sauropodomorph taxon *Wudingloong wui*[19]. These dinosaur remains are significant as they represent one of the earliest large-bodied herbivorous dinosaurs in the region, providing a key palaeontological anchor for our chemostratigraphic analysis. The Yubacun Formation records the demise of Late Triassic peat-forming environments and the shift towards Early Jurassic aridification environments, marked by an increased occurrence of calcareous components upwards (Fig. 1C & Figure S2). It archives the Kunming Basin's transition from humid Late Triassic to semi-arid Early Jurassic oxidative regimes, likely linked to Tethyan tectonism and global TJT palaeoclimatic as well as carbon cycle perturbations[64]. The succeeding Lower Jurassic Lufeng Formation comprises maroon mudstones interbedded with quartzose sandstones and common calcareous nodules, indicative of seasonal aridity, oxidizing lacustrine-fluvial settings that host abundant vertebrate fossils like *Lufengosaurus*[16,17].

Drill core WK23-1 (102°10'56" E, 26°03'30" N; Wande section, Fig. 1B), recovered from the site ~1 km away from the dinosaur fossil locality, spans the critical TJT interval and provides a continuous archive for investigating terrestrial responses to TJT events in the eastern Tethyan realm. Establishing a robust correlation between our drill core and the fossil site is fundamental. While diachroneity is a valid concern in any continental setting, our correlation is robustly supported by the ability to physically trace the key formational contact in the field, the consistency of the entire stratigraphic package, and the well-defined regional chronostratigraphy[63]: 1) The topography between the drill site and the fossil locality (~ 1 km apart) allows for the key stratigraphic contacts to be walked out. The most distinct of these is the sharp, conformable contact between the underlying grey-green sandstones of the Shezi Formation and the first appearance of the variegated (purple-red and grey-green) mudstones and sandstones of the

Yubacun Formation. This lithological boundary is a consistent and mappable surface in the study area and serves as our primary correlation datum. 2) The entire stratigraphic package, including the consistent nature of the underlying Shezi Formation (grey-green, thick-bedded sandstones), the characteristic lithology of the Yubacun Formation itself (stably variegated, and the consistent position below the overlying Lufeng Formation (purple-red thick-bedded sandstones and mudstones), is consistent with the well-established regional framework. This package represents a clear, basin-wide environmental transition from the humid, coal-forming conditions of the Late Triassic to the arid "red bed" environment of the Early Jurassic. 3) At present, no palynological data have been published from the Yubacun Formation in our specific study area. However, the Early Jurassic age of the formation regionally is well-constrained by invertebrate fossils (e.g., bivalves and gastropods) and palaeomagnetism (Hettangian to early Sinemurian).

The drill core and outcrop correlation was accomplished through lithology of the Yubacun Formation's variegated clastic characteristics and its thickness, confirming the dinosaur-bearing horizon occurs no shallower than the Shezi–Yubacun lithologic contact at 15.23 m within the core (Fig. 1C), and no deeper than the base of the greyish-green siltstone unit at 23.73 m.

Natural Gamma-Ray (GR) logging and astronomical tuning

To establish a high-resolution chronostratigraphic framework, natural gamma-ray (GR) logging was performed on core WK23-1 via wireline logging. Continuous GR measurements were acquired at 0.1 m vertical resolution. Assuming GR variations in this clastic succession primarily reflect changes in clay mineral content potentially driven by orbitally modulated climate cycles affecting weathering and sediment influx, we performed cyclostratigraphic analysis using the Acycle v2.8 software[65]. Temporal calibration was achieved through iterative orbital tuning, whereby the 405-kyr eccentricity cycle component of the La2010d astronomical solution[66] was phase-locked to the GR-derived sedimentary cycles. Detailed methodological protocols are provided in the Supplementary Materials.

Geochemical analysis

A total of 441 samples were collected from fine-grained lithologies (mudstone, siltstone) of drill core WK23-1, avoiding visible veins or significant alteration. The average sampling resolution was approximately 0.6 m. Samples were dried, crushed, and pulverized to ~200 mesh (< 75 μm) using a tungsten carbide mill for subsequent geochemical analyses.

Major and trace element concentrations were determined for 88 samples at the Wuhan Sample Solution Analytical Technology Co., Ltd. Major elements were measured by X-ray fluorescence spectrometer (XRF), and the analytical precision is better than ± 2–5% with certified reference material (GBW07103, GBW07105, GBW07108, GBW07111, and GBW07112) for analytical quality monitoring. Trace elements were measured by Agilent 7700e inductively coupled plasma mass spectrometry (ICP-MS). Accuracy and precision were monitored using certified reference materials BHVO-2 (basalt), RGM-2 (rhyolite), GSR-3, and JA-2 and replicate analyses. Bulk-rock major and trace element data are given in Supplementary Data S1.

A total of 246 samples were analyzed for TOC and $\delta^{13}C_{org}$. Prior to analysis, powdered samples were treated with dilute hydrochloric acid overnight to remove carbonate minerals, then rinsed with deionized water and dried. Approximately 1–10 mg of decarbonated powder was weighed into tin capsules for analysis. The initial analyses were performed at the Institute of Palaeontology, Yunnan University, using a Thermo Scientific Delta V Advantage. The linearity of this instrument is confirmed periodically and during each analytical run, a matrix-matched reference material (High Organic Sediment Standard OAS, IVA3380215) was analyzed every 10–15 samples to monitor and correct for instrument drift. To provide a final and definitive quality check, selected samples mainly from the three key CIE intervals were re-analyzed at the State Key Laboratory of Geological Processes and Mineral Resources, China University of Geosciences (Wuhan), using a MAT 253 IR-MS. The protocol for this new analysis included a formal two-point calibration to the V-PDB scale using international reference materials IAEA-600 (-27.771‰) and USGS40 (-26.39‰). These standards were analyzed at high frequency (two for every ten samples) to ensure stability, and the measured mean values for IAEA-600 (-27.79 ± 0.10‰, 1σ, n = 26) and USGS40 (-26.39 ± 0.09‰, 1σ, n = 30) were in excellent agreement with their accepted values. A linear correction was applied to all samples, and the overall analytical precision was better than 0.10‰ (1σ). Critically, the repeated measurements from both laboratories were comparable, confirming the accuracy and robustness of our results. All $\delta^{13}C_{org}$ measurements are reported relative to Vienna Pee Dee Belemnite (V-PDB). Additionally, replicate TOC contents were cross-validated on 120 samples using an Elementar vario Macro cube CNS Element Analyzer at the Institute of Palaeontology, Yunnan University.

Total Hg concentrations were determined for 434 samples using a Direct Mercury Analyzer (DMA-80 evo) at the Institute of Palaeontology, Yunnan University. Analytical accuracy was monitored using the certified reference material GBW07405a (GSS-5a, yellow-red soil, certified Hg = 700 ± 100 ng/g). Replicate analyses of GSS-5a yielded a relative standard deviation (RSD) better than 5% (2σ), confirming analytical precision. The Hg enrichment factor (Hg_{EF}) is calculated according to:

$$Hg_{EF} = \frac{(Hg/Al)_{sample}}{(Hg/Al)_{bg}} \quad (1)$$

where $(Hg/Al)_{sample}$ is the Hg/Al ratio of individual core sample, and $(Hg/Al)_{bg}$ is the background value (3.224 ppb/wt%) defined by the average Hg/Al ratios of samples from the interval below the P-CIE.

Ten samples exhibiting elevated Hg concentrations were selected for Hg isotope analysis. Mercury was liberated via pyrolysis and subsequently analyzed using a Nu-Plasma multi-collector inductively coupled plasma mass spectrometer (MC-ICP-MS) at the Institute of Geochemistry, Chinese Academy of Sciences, Guiyang, China. Instrumental drift was monitored by interspersing NIST SRM 3133 standard measurements after every three unknown samples. Mercury mass-dependent fractionation (MDF) is reported in delta notation (δ)[22,67]:

$$\delta^{202}Hg = \left[\left(\frac{^{202}Hg}{^{198}Hg} \right)_{sample} \Big/ \left(\frac{^{202}Hg}{^{198}Hg} \right)_{NIST\,3133} - 1 \right] \times 10^3 \quad (2)$$

Mass-independent fractionation (MIF) is quantified using capital delta notation (Δ) as the deviation from the theoretically predicted values by MDF laws:

$$\Delta^{xxx}Hg = \delta^{xxx}Hg - \beta \times \delta^{202}Hg \quad (3)$$

where xxx = 199, 200, or 201, and β-values are 0.252, 0.502, and 0.752 for isotopes ^{199}Hg, ^{200}Hg, and ^{201}Hg, respectively, following kinetic MDF law[35].

Chemical index of alteration

Palaeoweathering intensity was assessed using the Chemical Index of Alteration (CIA), calculated from major element oxide weight percentages: $CIA = [Al_2O_3 / (Al_2O_3 + CaO^* + Na_2O + K_2O)] \times 100$[68]. CaO* represents the CaO incorporated in the silicate fraction only, corrected following the methodology of ref. 69. Higher CIA values generally indicate more intense chemical weathering, since this proxy effectively tracks the decomposition of labile minerals (e.g., plagioclase) relative to weathering-resistant phases (e.g., clays)[70–72].

Data availability

All data are available in the main text or the supplementary materials.

Received: 21 May 2025; Accepted: 1 December 2025;
Published online: 13 January 2026

References

1. Schoepfer, S. D., Algeo, T. J., van de Schootbrugge, B. & Whiteside, J. H. The Triassic–Jurassic transition – A review of environmental change at the dawn of modern life. *Earth-Science Reviews* **232**, 104099 (2022).
2. McElwain, J. C., Beerling, D. J. & Woodward, F. I. Fossil plants and global warming at the Triassic-Jurassic boundary. *Science* **285**, 1386–1390 (1999).
3. McHone, J. G. Volatile emissions from Central Atlantic Magmatic Province Basalts: Mass assumptions and environmental consequences. In *Geophysical Monograph* Vol. 136 (2003).
4. van De Schootbrugge, B. et al. Floral changes across the Triassic/Jurassic boundary linked to flood basalt volcanism. *Nature Geosci* **2**, 589–594 (2009).
5. Zhang, P. et al. Significant floral changes across the Permian-Triassic and Triassic-Jurassic transitions induced by widespread wildfires. *Front Ecol Evol* **11**, 1284482 (2023).
6. Brusatte, S. L., Benton, M. J., Ruta, M. & Lloyd, G. T. Superiority, competition, and opportunism in the evolutionary radiation of dinosaurs. *Science* **321**, 1485–1488 (2008).
7. Benton, M. J. The origins of modern biodiversity on land. *Phil. Trans. R. Soc. B* **365**, 3667–3679 (2010).
8. Olsen, P. E. et al. Ascent of dinosaurs linked to an iridium anomaly at the Triassic-Jurassic boundary. *Science* **296**, 1305–1307 (2002).
9. Olsen, P. et al. Arctic ice and the ecological rise of the dinosaurs. *Sci. Adv.* **8**, eabo6342 (2022).
10. Upchurch, P. & Chiarenza, A. A. A brief review of non-avian dinosaur biogeography: state-of-the-art and prospectus. *Biol. Lett.* **20**, 20240429 (2024).
11. Hesselbo, S. P., Robinson, S. A., Surlyk, F. & Piasecki, S. Terrestrial and marine extinction at the Triassic-Jurassic boundary synchronized with major carbon-cycle perturbation: A link to initiation of massive volcanism? *Geology* **30**, 251–254 (2002).
12. Ruhl, M., Kürschner, W. M. & Krystyn, L. Triassic–Jurassic organic carbon isotope stratigraphy of key sections in the western Tethys realm (Austria). *Earth Planet. Sci. Lett.* **281**, 169–187 (2009).
13. Thibodeau, A. M. et al. Mercury anomalies and the timing of biotic recovery following the end-Triassic mass extinction. *Nat. Commun.* **7**, 11147 (2016).
14. Lindström, S. et al. Volcanic mercury and mutagenesis in land plants during the end-Triassic mass extinction. *Sci. Adv.* **5**, eaaw4018 (2019).
15. Lindström, S. et al. Tracing volcanic emissions from the Central Atlantic Magmatic Province in the sedimentary record. *Earth-Sci. Rev.* **212**, 103444 (2021).
16. C. C. Young, *The Lufeng Saurischian Fauna in China* (1951)vol. 13 of *Palaeontologica Sinica*, *New Series C*.
17. Zhang, Q.-N., Jia, L., Wang, T., Zhang, Y.-G. & You, H.-L. The largest sauropodomorph skull from the Lower Jurassic Lufeng Formation of China. *PeerJ* **12**, e18629 (2024).
18. Zou, Y. et al. A new metriacanthosaurid theropod dinosaur from the Middle Jurassic of Yunnan Province, China. *PeerJ* **13**, e19218 (2025).
19. Wang, Y.-M. et al. A new Early Jurassic dinosaur represents the earliest-diverging and oldest sauropodomorph of East Asia. *Scientific Reports* **15**, 26749 (2025).
20. Whiteside, J. H. et al. Extreme ecosystem instability suppressed tropical dinosaur dominance for 30 million years. *Proc. Natl. Acad. Sci. USA.* **112**, 7909–7913 (2015).
21. Xing, L.-D. et al. Late Triassic sauropodomorph and Middle Jurassic theropod tracks from the Xichang Basin, Sichuan Province, southwestern China: First report of the ichnogenus Carmelopodus. *Journal of Palaeogeography* **7**, 1–13 (2018).
22. Grasby, S. E., Them II, T. R., Chen, Z., Yin, R. & Ardakani, O. H. Mercury as a proxy for volcanic emissions in the geologic record. *Earth-Sci. Rev.* **196**, 102880 (2019).
23. Ruhl, M. et al. On the onset of Central Atlantic Magmatic Province (CAMP) volcanism and environmental and carbon-cycle change at the Triassic–Jurassic transition (Neuquén Basin, Argentina). *Earth-Sci. Rev.* **208**, 103229 (2020).
24. Suarez, C. A. et al. A revised chronostratigraphy of the Triassic-Jurassic Moenave Formation, western USA: Implications for timing of continental climate change. *GSA Bulletin* **137**, 5009–5027 (2025).
25. Whiteside, J. H., Olsen, P. E., Eglinton, T., Brookfield, M. E. & Sambrotto, R. N. Compound-specific carbon isotopes from Earth's largest flood basalt eruptions directly linked to the end-Triassic mass extinction. *Proc. Natl. Acad. Sci. USA.* **107**, 6721–6725 (2010).
26. Yager, J. A. et al. Duration of and decoupling between carbon isotope excursions during the end-Triassic mass extinction and Central Atlantic Magmatic Province emplacement. *Earth Planet Sc Lett* **473**, 227–236 (2017).
27. Deenen, M. H. L. et al. A new chronology for the end-Triassic mass extinction. *Earth and Planetary Science Letters* **291**, 113–125 (2010).
28. Chen, J. et al. Regional postdeforestation weathering feedback drove diachronous C–S cycle perturbations during the end-Permian crisis. *Proc. Natl. Acad. Sci. USA.* **122**, e2504841122 (2025).
29. Schubert, B. A. & Hope Jahren, A. Reconciliation of marine and terrestrial carbon isotope excursions based on changing atmospheric CO2 levels. *Nat Commun* **4**, 1653 (2013).
30. Fang, Y. et al. Carbon isotope stratigraphy across the Triassic-Jurassic boundary in the high-latitude terrestrial Junggar Basin, NW China. *Palaeogeography, Palaeoclimatology, Palaeoecology* **577**, 110559 (2021).
31. Wotzlaw, J.-F. et al. Towards accurate numerical calibration of the Late Triassic: High-precision U-Pb geochronology constraints on the duration of the Rhaetian. *Geology* **42**, 571–574 (2014).
32. Caruthers, A. H. et al. New evidence for a long Rhaetian from a Panthalassan succession (Wrangell Mountains, Alaska) and regional differences in carbon cycle perturbations at the Triassic-Jurassic transition. *Earth Planet. Sci. Lett.* **577**, 117262 (2022).
33. S. P. Hesselbo, J. G. Ogg, M. Ruhl, L. A. Hinnov, C. J. Huang, "The Jurassic Period" in *Geologic Time Scale 2020* (Elsevier, 2020; https://linkinghub.elsevier.com/retrieve/pii/B9780128243602000267), pp. 955–1021.
34. Chen, J. et al. Spatiotemporal disparity of volcanogenic mercury records in the southwestern Neo-Tethys Ocean during the Permian–Triassic transition. *Global Planet. Change* **240**, 104534 (2024).
35. Blum, J. D., Sherman, L. S. & Johnson, M. W. Mercury Isotopes in Earth and Environmental Sciences. *Annu. Rev. Earth Planet. Sci.* **42**, 249–269 (2014).
36. Yager, J. A. et al. Mercury contents and isotope ratios from diverse depositional environments across the Triassic–Jurassic Boundary: Towards a more robust mercury proxy for large igneous province magmatism. *Earth-Sci. Rev.* **223**, 103775 (2021).
37. Paris, G., Donnadieu, Y., Beaumont, V., Fluteau, F. & Goddéris, Y. Geochemical consequences of intense pulse-like degassing during the onset of the Central Atlantic Magmatic Province. *Palaeogeography, Palaeoclimatology, Palaeoecology* **441**, 74–82 (2016).
38. Beith, S. J., Fox, C. P., Marshall, J. E. A. & Whiteside, J. H. Compound-specific carbon isotope evidence that the initial carbon isotope excursion in the end-Triassic strata in northwest Tethys is not the product of CAMP magmatism. *Global Planet Change* **222**, 104044 (2023).
39. Lei, J. Z. X. et al. Late Triassic carbon isotope anomalies in the Canadian Cordillera: Paleoenvironmental disturbances associated with the Norian/Rhaetian boundary and end-Triassic mass extinction event. *Global and Planetary Change* **242**, 104563 (2024).
40. Ruhl, M. & Kürschner, W. M. Multiple phases of carbon cycle disturbance from large igneous province formation at the Triassic-Jurassic transition. *Geology* **39**, 431–434 (2011).
41. Li, L., Wang, Y., Kürschner, W. M., Ruhl, M. & Vajda, V. Palaeovegetation and palaeoclimate changes across the Triassic–Jurassic transition in the Sichuan Basin, China. *Palaeogeogr Palaeocl*. **556**, 109891 (2020).

42. Bos, R. et al. Climate-forced Hg-remobilization associated with fern mutagenesis in the aftermath of the end-Triassic extinction. *Nat Commun*. **15**, 3596 (2024).
43. Shen, J., Yin, R., Algeo, T. J., Svensen, H. H. & Schoepfer, S. D. Mercury evidence for combustion of organic-rich sediments during the end-Triassic crisis. *Nat. Commun.* **13**, 1307 (2022).
44. Chen, J. et al. Inconsistent mercury records from terrestrial upland to coastal lowland across the Permian-Triassic transition. *Earth Planet. Sci. Lett.* **614**, 118195 (2023).
45. Percival, L. M. E. et al. Mercury evidence for pulsed volcanism during the end-Triassic mass extinction. *Proc. Natl. Acad. Sci. USA.* **114**, 7929–7934 (2017).
46. Zhou, Y. et al. The role of LIPs in Phanerozoic mass extinctions: An Hg perspective. *Earth-sci Rev* **249**, 104667 (2024).
47. Shen, J. et al. Intensified continental chemical weathering and carbon-cycle perturbations linked to volcanism during the Triassic–Jurassic transition. *Nat. Commun.* **13**, 299 (2022).
48. Xing, K.-C. et al. High-latitude climatic response across the Triassic-Jurassic boundary recorded by Mg-Cu-Zn isotopes. *Chemical Geology* **610**, 121085 (2022).
49. Wan, R. et al. Intensified continental weathering and reductive surface runoff during the Triassic−Jurassic transition. *Geology* **53**, 13–17 (2024).
50. Li, X. et al. Early Jurassic climate and atmospheric CO2 concentration in the Sichuan paleobasin, southwestern China. *Clim. Past* **16**, 2055–2074 (2020).
51. Heath, J. A., Cooper, N., Upchurch, P. & Mannion, P. D. Accounting for sampling heterogeneity suggests a low paleolatitude origin for dinosaurs. *Current Biology* **35**, 941–953.e5 (2025).
52. Chiarenza, A. A. et al. Early Jurassic origin of avian endothermy and thermophysiological diversity in dinosaurs. *Current Biology* **34**, 2517–2527 (2024).
53. Qvarnström, M. et al. Digestive contents and food webs record the advent of dinosaur supremacy. *Nature* **636**, 397–403 (2024).
54. Scotese, C. R. An atlas of Phanerozoic paleogeographic maps: The seas come in and the seas go out. *Annu. Rev. Earth Planet. Sci.* **49**, 679–728 (2021).
55. Apaldetti, C., Pol, D., Ezcurra, M. D. & Martínez, R. N. Sauropodomorph evolution across the Triassic–Jurassic boundary: body size, locomotion, and their influence on morphological disparity. *Sci Rep*. **11**, 22534 (2021).
56. Dunne, E. M. et al. Climatic controls on the ecological ascendancy of dinosaurs. *Current Biology* **33**, 206–214 (2023).
57. Song, Y. et al. Distribution of pyrolytic PAHs across the Triassic-Jurassic boundary in the Sichuan Basin, southwestern China: Evidence of wildfire outside the Central Atlantic Magmatic Province. *Earth-sci Rev* **201**, 102970 (2020).
58. Fox, C. P., Holman, A. I., Rigo, M., Al Suwaidi, A. & Grice, K. Paleowildfire at the end-Triassic mass extinction: Smoke or fire? *Global Planet Change* **218**, 103974 (2022).
59. L. H. Tanner, Ed., *The Late Triassic World: Earth in a Time of Transition* (Springer International Publishing, 2018; http://link.springer.com/10.1007/978-3-319-68009-5)vol. 46 of *Topics in Geobiology*.
60. Judd, E. J. et al. A 485-million-year history of Earth's surface temperature. *Science* **385**, eadk3705 (2024).
61. Zhang, P. et al. Volcanically-induced environmental and floral changes across the Triassic-Jurassic (T-J) transition. *Front. Ecol. Evol.* **10**, 853404 (2022).
62. Feng, Z. et al. Evidence for insect-mediated skeletonization on an extant fern family from the Upper Triassic of China. *Geology* **42**, 407–410 (2014).
63. Xiaosi Fang et al, *The Jurassic Red Bed in the Central Yunnan of China* (Geological Publishing House, Beijing, 2008).
64. Blackburn, T. J. et al. Zircon U-Pb geochronology links the End-Triassic extinction with the Central Atlantic Magmatic Province. *Science* **340**, 941–945 (2013).
65. Li, M., Hinnov, L. & Kump, L. Acycle: Time-series analysis software for paleoclimate research and education. *Computers & Geosciences* **127**, 12–22 (2019).
66. J. Laskar, "Astrochronology" in *Geologic Time Scale 2020* (Elsevier, 2020; https://linkinghub.elsevier.com/retrieve/pii/B9780128243602000048), pp. 139–158.
67. Chen, J., Hintelmann, H., Feng, X. & Dimock, B. Unusual fractionation of both odd and even mercury isotopes in precipitation from Peterborough, ON, Canada. *Geochim. Cosmochim. Acta* **90**, 33–46 (2012).
68. Nesbitt, H. W. & Young, G. M. Early Proterozoic climates and plate motions inferred from major element chemistry of lutites. *Nature* **299**, 715–717 (1982).
69. McLennan, S. M. Weathering and global denudation. *The Journal of Geology* **101**, 295–303 (1993).
70. Yang, J., Cawood, P. A., Du, Y., Li, W. & Yan, J. Reconstructing Early Permian tropical climates from chemical weathering indices. *Geological Society of America Bulletin* **128**, 739–751 (2016).
71. Dinis, P. A., Garzanti, E., Hahn, A., Vermeesch, P. & Cabral-Pinto, M. Weathering indices as climate proxies. A step forward based on Congo and SW African river muds. *Earth-Science Reviews* **201**, 103039 (2020).
72. Chen, J. et al. Evaluation of chemical weathering proxies by comparing drilled cores versus outcrops and weathering history during the Permian–Triassic transition. *Global Planet. Change* **214**, 103855 (2022).
73. Hua, X. et al. Mercury isotope constraints on the timing and pattern of magmatism during the end-Triassic mass extinction. *Earth Planet Sc Lett*. **624**, 118438 (2023).
74. Fox, C. P. et al. Molecular and isotopic evidence reveals the end-Triassic carbon isotope excursion is not from massive exogenous light carbon. *Proc. Natl. Acad. Sci. USA.* **117**, 30171–30178 (2020).
75. A. Marzoli et al, "The Central Atlantic Magmatic Province (CAMP): A Review" in *The Late Triassic World* (Springer International Publishing AG., 2018) *Topics in Geobiology*, pp. 91–125.

Acknowledgements

Mr. Xiong Mo from the Yunnan Institute of Geological Survey, Dr. Huan Xu and Dr. Huanyu Liao from Yunnan University are thanked for their assistance during the field work and for generating the lithological column of the Wande outcrop. The Editors, three reviewers (Prof. Chris Griffin, Prof. Celina Suarez, and one anonymous reviewer) are appreciated for their time, expertise, and constructive guidance, which greatly improved the paper. This study was supported jointly by the National Natural Science Foundation of China (42325201; 42572030; 42372030), the Yunnan Province Science and Technology Department (202302AO370014), Yunnan Science & Technology Champion Project (202305AB350006), and the Scientific Research Fund Project of Yunnan Education Department (2025Y0021).

Author contributions

J.C., H.L.Y., X.X., S.Z.S., and Z.F. conceptualized and designed the research. J.C. and R.M. were responsible for core logging and completed the astronomical tuning. Sample preparation and subsequent analyses were performed by J.C., Y.N.N., Y.L.Z., and W.J.L. J.C. wrote the draft with substantial inputs from Y.M.W., H.L.Y., X.X., and Z.F. All coauthors contributed to the data analysis and the writing of the manuscript.

Competing interests

The author declares no competing interests.

Additional information

Supplementary information The online version contains supplementary material available at https://doi.org/10.1038/s43247-025-03083-6.

Correspondence and requests for materials should be addressed to Zhuo Feng.

Peer review information *Communications Earth and Environemnt* thanks Celina A. Suarez and the other, anonymous, reviewer(s) for their contribution to the peer review of this work. Primary Handling Editors: Yuan Shang and Alireza Bahadori. A peer review file is available.

Reprints and permissions information is available at http://www.nature.com/reprints

Publisher's note Springer Nature remains neutral with regard to jurisdictional claims in published maps and institutional affiliations.